Residual Stress-Driven Delamination in Deposited Multi-Layers

J.L. Beuth, S.H. Narayan

EDRC 24-118-95

Residual Stress-Driven Examination in Deposited Multi-Layers

J.L. Beuth
Department of Mechanical Engineering
Carnegie Mellon University
Schenley Park
Pittsburgh, PA 15213

S.H. Narayan
Department of Mechanical Engineering
Carnegie Mellon University
Schenley Park
Pittsburgh, PA 15213

Abstract

An analysis is presented of the problem of residual stress-driven delamination in materials or parts manufactured by successive layer deposition. A direct application of this work is to parts that are built using rapid prototyping-based layered manufacturing methods. A two-dimensional model is presented that allows calculation of steady-state energy release rates for delamination cracks. Results from a finite element model of the problem are also presented The results verify the steady-state analysis and show that it is applicable over a wide range of part dimensions. Crack displacement modes are also extracted from the finite element model. Results are presented for two and four layer bi-material configurations, over a large range of material mismatches. Examples are given of how this work can be used to identify critical interfaces where delamination is most likely to occur and to thus predict the susceptibility of multi-layers to delamination.*

***This work has been supported by the Engineering Design Research Center, a NSF Engineering Research Cento.**

Introduction and Problem Statement

This study addresses the problem of residual stress-driven delamination or debonding between successively deposited isotropic material layers. Results from this work can be applied to delamination problems associated with any process involving the successive deposition of material layers at elevated temperatures, such as multi-layered films or coatings. Methods outlined in this study can also be applied to debonding problems in laminated isotropic layers subjected to thermal mismatch stresses due to a temperature change. The type of application serving as the motivation for this work is the problem of residual stress-driven delamination in parts made by rapid prototyping-based layered manufacturing methods. Such methods involve the automated manufacture of three-dimensional parts by successive layering, starting with a three-dimensional CAD representation of part geometry. The aim of research into these methods is to extend rapid prototyping concepts to allow the manufacture of functional prototypes and/or production-quality parts.

The particular layered manufacturing method motivating this work has been termed shape deposition. Shape deposition is a process by which three-dimensional shapes or parts are built up incrementally by the successive application of molten material (primarily metal) layers. The process allows the deposition of single or multiple materials as needed. Shape deposition involves three major steps. In the first step, a three-dimensional CAD model is made of the shape to be created. In the second step, this model is numerically divided into layers and deposition and machining steps are programmed. The final step consists of the repeated application and CNC machining of layers of the part itself and also layers of support material. The support material, which is removed after the part is completed, is deposited around the part as it is being built and helps to maintain part shape. The deposition method currently used in this process has been termed microcasting. In microcasting, material is deposited in the form of molten metal droplets. The diameter of microcasted droplets is comparable to the layer thickness, which is typically on the order of 1.5 mm or more. Practical applications of shape deposition are directed toward the automated manufacture of parts of one or more materials, parts produced in small quantities and/or parts with complex internal geometries. A complete description of shape deposition is given by Merzetal.(1994).

An inherent complication associated with this process is the build-up of residual thermal stresses as new layers are deposited onto existing layers of the part. This is due to the free thermal contraction newly deposited material experiences as it solidifies and cools. Residual stresses can cause delaminations between layers by acting as the driving force in the extension of interfacial cracks from the edges of the part toward its center. A delamination may propagate through the entire length of the part, separating it into two pieces. One objective of this study is to quantify the susceptibility of shape deposited parts (and deposited multi-layers in general) to residual stress-

driven delamination. Another objective is to formulate simple delamination models that can guide the design of delamination-resistant parts.

Delamination is one of the principal sources of failure in laminated composites. As a result, there exists a large amount of work on composite delamination in the literature. A full account of previous work in this area is not provided here; however, approaches to the problem tend to fall into one of two categories. In the first category, the stresses along an uncracked interface are used as the basis for predicting delamination susceptibility. One approach of this type has been to formulate approximate stress distributions near the free edge to compare the delamination resistance of various laminate configurations (e.g., Whitney (1973) and Pagano and Pipes (1973)). A second approach in this category has involved use of finite element modeling to study the details of the elastic stress distributions near the free edge, with insights offered as to which stresses may be singular (e.g., the work on thermally induced stresses by Herakovich (1976) and Crossman and Wang (1977)). The second category of approaches to the composite delamination problem involves using fracture mechanics and calculating energy release rates of delamination cracks as a function of crack length. This approach is preferable because, unlike stress-based approaches, it avoids (without ignoring) difficulties associated with the stress singularities at the intersection of a free edge and a fully bonded interface (see Bogy (1971) or Hein and Erdogan (1971) (for isotropic layers) or Wang and Choi (1982) (for anisotropic layers)). Wang (1982,1984) took this approach in studying delaminations in composites under axially applied loads. O'Brien (1982) and O'Brien, Raju and Garber (1986) also used this approach by comparing strain energy release rates associated with delamination.

The approach taken in this study is to model the delamination problem in deposited multi-layers as an interfacial fracture mechanics problem. In the next section, a simple model based on steady-state cracking is formulated for predicting energy release rates for long delamination cracks. Previous models of this type have only been applied to problems of single thin films debonding from thick substrate materials. In the section following the next, a finite element model is presented for rigorously determining the limits of the simple model and for extracting crack extension modes. Results from both models are presented in the final section. These offer a full accounting of the multi-layer residual stress-driven delamination problem.

Steady-State Delamination Model

In this section, a steady-state two-dimensional fracture mechanics-based delamination model is presented. Figure 1 illustrates a delamination crack that has initiated at a free edge and is propagating along the mid-plane interface of a four-layer part. The crack front is straight and perpendicular to both the x and y axes. It is assumed that material in each layer has experienced a free thermal contraction with respect to the layer below it and that this contraction is independent of the x-coordinate. Under this assumption, the potential energy released by extending the crack a

fixed distance in the x direction reaches a steady-state (constant in magnitude) value for a crack of sufficient length. It is this potential energy release, expressed in the form of an energy release rate, which acts as a driving force in extending a delamination crack.

By definition, the energy release rate, G, is the potential energy released per unit newly created crack surface, defined by the relation

$$-\frac{\partial PE}{\partial a} \qquad (1)$$

where PE is the potential energy in the part, B is the part width and a is the crack length. For a sufficiently long delamination crack, the steady-state energy release rate, G_{ss}, can be calculated as the difference in the potential energy per unit width per unit length between a fully bonded four-layer part and a part that has been separated into two two-layer pieces. The physical reasoning behind this model is that for a sufficiently long crack, the near-crack-tip stress distribution simply translates in the x-direction as the crack extends. Under such conditions, the potential energy released by extending the crack a unit distance in the x direction is the difference in potential energy between unit length portions of the part far ahead and far behind the crack tip. A consequence of this steady-state condition is that a solution that models the near-crack-tip fields is not needed in order to calculate G_{ss} of the delamination crack. Instead, a model of the residual stress state in each layer of an uncracked multi-layer can be used. The residual stress model also does not need to model stresses near the ends of each layer.

This approach (which represents a significant simplification of the problem) is based on the concept of steady-state cracking as articulated in the review article by Hutchinson and Suo (1991). The key point of this concept is that many cracking problems in multi-layered materials reach configurations where the crack driving force becomes independent of crack length. It is often this final value of the crack driving force which controls the physical cracking behavior. A principal goal of this study is to use values of G_{SS} to predict the susceptibility of a given interface to delamination. If the critical energy release rate for propagation along the interface, G_c, is greater than G_{SS}, then no delamination will occur. The work in the literature most closely related to that presented here is the work of O'Brien (1982) and O'Brien, Raju and Garber (1986) on the delamination problem in laminated fibrous composite materials. Their work used the energy released in dividing a laminate into "sublaminates" to calculate the energy release rate of delamination cracks in axially loaded and thermally loaded graphite-epoxy coupons. Additionally, the steady-state concept has been used in studies of a single thin film debonding from a thick substrate material by Drory, Thouless and Evans (1988), Evans, Drory and Hu (1988) and Thouless, Cao and Mataga (1989).

In this study, a simple model of residual stress build-up is used which is based on the solution by Timoshenko (1925) for the stresses in a uniformly heated bi-material strip. The current model is a generalization of the Timoshenko model to any number of layers. It is assumed that

each layer experiences a uniform free thermal contraction (characterized by an a AT) relative to the layer below it. As in the model of Timoshenko, the layers behave as beams with linear variations of stress in the y direction (see Fig. 1) in each layer. All results presented in this study assume global plane stress conditions. They are therefore directly applicable to parts or portions of parts that are thin in the direction normal to the x and y axes. A consequence of this assumption is that all calculated energy release rates are independent of material Poisson's ratios. By using the appropriate formula to convert energy release rates to stress intensity factors (look ahead to eq. (7)), plane stress or plane strain conditions can be modeled near the crack tip. The results presented in this study can also be applied to delamination problems in thick parts, where each layer is in a global state of biaxial tension. This can be done by substituting E/(1-v) for E and multiplying energy release rate values by a factor of two (corresponding to two stresses of equal magnitude being released by the extension of the delamination crack). It is also assumed that all layers are deposited and have cooled to room temperature before any bending deformation takes place. This final assumption models a multi-layer which is fully constrained from bending deformation during its construction. Although it is not addressed in this study, an analogous residual stress model can be constructed without a bending constraint The constrained condition is studied here because it more closely models the actual constraint conditions applied to shape deposited parts during their manufacture. This constraint is provided by the surrounding support material and the base upon which the part is built.

The current residual stress model serves as a first-step approach to modeling the delamination problem in multi-layers, which does not fully account for all of the characteristics of the shape deposition process to which it is being applied. For example, the current model cannot accurately predict residual stress magnitudes in shape deposited parts, since these are a function of high-temperature creep and yield behavior and the temperature dependence of properties such as the elastic moduli and the coefficient of thermal expansion, a. The model also does not account for nonuniform contraction in the thickness direction within individual layers in shape deposition processes. For example, in the microcasting process, each droplet solidifies essentially from the bottom up. A droplet-level solidification model with temperature dependent properties is under development that will account for these effects. The current model can be used directly as a means for comparison between some shape deposited configurations. It will also serve as a basis for comparison with future work based on more refined residual stress models.

In summary, a steady-state analytical delamination model is presented which involves calculation of the energy release rate for delamination cracks in multi-layers using a simple residual-stress model. The goal of this work is to use the insight offered by a simple model to formulate design guides for minimizing the steady-state energy release rate for delamination cracks and to thus decrease the likelihood that delaminations will occur in multi-layered parts or materials. In the

next section, a finite element analysis is presented which is used to verify the steady-state concept and to extract crack tip opening and sliding modes, which can only be extracted from a fracture analysis of the problem.

Finite Element Model

The steady-state delamination model just outlined is sufficient to calculate values of Gss for any layered configuration. However, a fracture mechanics-based model of the problem is also needed. Although it is apparent that a constant energy release rate is reached for a sufficiently long crack, it is not known how long a delamination crack must be in order for steady-state conditions to apply. It is also not known what dimensions of parts can be modeled by a beam-based steady-state model. The steady-state delamination model also does not ensure that G_{ss} is the maximum energy release rate for all crack lengths. A fracture model is therefore needed to evaluate the reasonableness of designing multi-layers based on values of Gss compared to values for G_c, the critical energy release rate for interfacial crack propagation. Finally, the mode of crack extension must be extracted from a fracture mechanics model of the problem. This is required in order to compare Gss values with mode-dependent G_c values from interfacial toughness tests.

The method of mode separation used in this study is one outlined by Matos et al (1989) for separating modes in interfacial fracture problems. Definitions for stress intensity factors and near-tip stress fields follow those given by (among others) Rice (1988) and Suo and Hutchinson (1990). The singular stress field just ahead of an interfacial crack tip (along 0 = 0) takes the following form:

$$cx^{\wedge}+ia_{xy}=K(2/nrV, \qquad (2)$$

where for materials 1 and 2 (see Fig. 1)

$$\varepsilon = \frac{1}{2\pi}\ln\left[\frac{\mu_1 + \mu_2\kappa_1}{\mu_2 + \mu_1\kappa_2}\right] \qquad (3)$$

and K = Ki+iK2 is the complex stress intensity factor for interfacial crack problems. In (3) |ij (j=l,2) is the material shear modulus and Kj = (3-Vj)/(l+Vj) (j=l,2) for plane stress and Kj = 3-4VJ (j=l,2) for plane strain. K, the complex stress intensity factor, takes the form

$$K = K_x + iK_2 = f \text{ x (applied stress) x } (V\overline{h}h\sim^{i\pounds}), \qquad (4)$$

where f is nondimensional and, in general, a complex function of the material properties and the specimen geometry. The parameter h is the characteristic length of the problem. For a steady-state delamination crack between layers of equal thickness, the characteristic length is the layer thickness, h.

The method used to extract the modes of crack extension from the finite element delamination models involves fitting the near-tip crack displacements from the model to the near-tip "K-field" opening and crack sliding displacements §2 and 8i given by

$$\delta_2 + i\delta_1 = \frac{1}{2}\left[\frac{C_1 + C_2}{(1+2i\varepsilon)\cosh(\pi\varepsilon)}\right] K \left(\frac{r}{2\pi}\right)^{1/2} r^{i\varepsilon}, \quad (5)$$

where Cj = (Kj4-l)/(jj 0=1,2). The mode of crack extension is defined by the phase angle, y, of the complex stress intensity factor K (see eq. (4)) defined by the equation

$$\psi = \tan^{-1}\left[\frac{\mathrm{Im}(Kh^{i\varepsilon})}{\mathrm{Re}(Kh^{i\varepsilon})}\right], \quad (6)$$

where y is defined to be independent of the characteristic length, h. For a unit value of h, \\f = 0° corresponds to pure Ki and *f* = 90° corresponds to pure K2. Inspection of eq. (2) reveals that *f* represents the ratio of normal to shear stresses ahead of the crack tip separated from the quantity $(r/h)^{ie}$. As eq. (5) illustrates, the correlation of \\f with the relative amounts of crack face opening and sliding displacements is less direct, due to the additional complex factor (l+2ie). In order to extract a value of y for a given problem, crack face displacements from the finite element solution at various distances from the crack tip are substituted into eq. (5). The complex K is solved for and values of \\/ are obtained using eq. (6). At each point where \\f is determined, the energy release rate, G, is also calculated from the displacements using the formula for conversion between GandK:

$$G = |K|^2\left[\frac{C_1 + C_2}{16\cosh^2 OOJ}\right] \quad (7)$$

The value of \\f is taken at the node location that agrees best with an independently evaluated J integral calculation of G (see Matos et. al (1989) for a discussion of the accuracy of this method).

An example of the finite element model used in this study is shown in Fig. 2. The model is constructed out of eight-noded plane stress quadrilateral interpolation elements using the finite element package ABAQUS. Thus, values of the energy release rate extracted from this model are for global plane stress conditions. Plane stress or plane strain conditions near the crack tip can be modeled by using the appropriate form of eq. (7) for converting the energy release rates to stress intensity factors. The vertical edge on the right side of the model is a line of symmetry. A refined mesh consisting of quarter-point elements is used near the crack tip to capture the 1/Vr near-tip strain dependence. The density of the near-tip mesh was varied to check for convergence; however, for the results presented here, the near-tip mesh consists of 18 rings of elements meshed over a length equal to h/2.

Results and Discussion

In this section, results from the steady-state delamination model and the finite element model are presented. Methods are also demonstrated for using the results to predict delamination resistance of multi-layered materials or parts. Energy release rates as a function of crack length are extracted from the finite element analysis by evaluation of a J integral. In Fig. 3, a plot of

normalized energy release rate vs. normalized crack length is given for the simplest case of delamination of a two-layer part with equal layer thicknesses and with both materials having equal elastic properties. The crack lengths are normalized with respect to the layer thickness, h. The half-length of the symmetric model is equal to 25 layer thicknesses in this case. Energy release rates for this and all other problems presented in this study are normalized with respect to the steady-state energy release rate for this problem. Because the debonded portion of the part is stress free for two-layer problems, the energy release rate is the strain energy per unit width per unit length in the fully bonded part, given by

$$G_0 = \wedge \quad (\alpha\Delta T)_g \, EH \quad , \qquad (8)$$

where H is the total thickness of the part under consideration, ocAT is the free thermal strain mismatch between the layers under consideration, and for this particular case $E_{av}g$ is simply the Young's modulus of the two materials. Subsequent (multi-material) problems are normalized using an Eavg which is a rule of mixtures Young's modulus defined as Eavg = £ Eihi / H. In this way, all energy release rates are normalized with respect to the energy release rate for a single material, two-layer part that is experiencing debonding along its midplane.

The plot provided in Fig. 3 demonstrates the steady-state nature of this problem. A steady-state value of G is rapidly reached (for a crack length of approximately one layer thickness or greater). This value is maintained until the symmetrically extending cracks have almost completely extended through the part. The steady-state values from the finite element analysis are also accurately predicted by the analytical steady-state model. As the plot in Fig. 3 indicates, if the critical energy release rate, G_c, for this interface is greater than G_{SS}, then no delamination crack extension will occur regardless of initial flaw size.

Figure 4 gives a plot of normalized G vs. a/h for the case of debonding of a two-layer part with the bottom layer having a stiffness that is three times that of the top layer. Additionally, symmetric model half-lengths of L = 15h and L = 25h are considered. Again, the steady-state nature of the problem is confirmed. Additionally, the short crack and long crack variations of energy release rate with crack length are independent of the total length of the part For the case of a short crack, the behavior is unaffected by extra bonded material far ahead of the crack tip. Similarly, for the case of a long crack, the energy release rate is unaffected by the amount of stress-free material far behind the crack tip. This also sets a limit for values of normalized part length L/h for which a beam-based steady-state analysis of this problem is valid. Because the short crack G vs. a curve rises to the steady-state value over a length of approximately one layer thickness, h, and the long crack steady-state curve falls from the steady-state value to zero over a length of approximately 2h, it is reasonable to conclude that the steady-state G is reached by any part having a normalized half-length L/h ≥ 3. Furthermore, for values of L/h < 3 a design based on setting $G_c > G_{SS}$ will be conservative, because G_{SS} will not be reached by the delamination crack.

Figure 5 provides a plot of normalized G vs. a/h for the case of a two-layer part and the case of a bottom layer having a stiffness that is 40 times that of the top layer. Again, a predictable steady-state value of G is achieved for crack lengths equal to approximately one layer thickness. The high stiffness mismatch causes the fall-off in G values for long cracks to occur over a length of approximately 3h. Thus, for this case the steady-state analysis applies for $L/h \geq 4$ and the method is conservative for $L/h < 4$. The results in Fig. 5 are also of importance because in this case (as in the cases shown thus far) Gss is the maximum energy release rate achieved for any crack length. As previously mentioned, this is by no means guaranteed. In fact, because a singularity in stresses exists at the intersection of the interface and the free edge for the case of an uncracked interface, there is potential for a local maximum in G to exist for short cracks.. Small delamination cracks initiating at the free edge are surrounded by a concentrated stress field. This could lead to large values of G for short delamination crack lengths. The strength of the singularity for the uncracked problem is greatest for cases with large stiffness mismatches. No short crack maximum in G is evident, however, even in the case of a stiffness mismatch of 1:40.

A critical issue in this work is how Gss values can be used to predict the susceptibility of a deposited multi-layer to delamination. In particular, it is of interest to determine whether simple changes in part design can increase delamination resistance. -Figure 6 provides an illustration of two two-layer part "designs." In design #1 a compliant layer is deposited onto a stiff layer. In design #2 a stiff layer is deposited onto a compliant layer. Arrows in the figure represent the direction of relative expansion/contraction of the deposited layer. The question addressed in Fig. 6 is whether one "design" is better than the other with respect to its delamination resistance. For the sake of comparison, it is assumed that the mismatch in free thermal strain between layers in both parts is the same. The following symmetry arguments can be used to show that the two part designs are related. In Fig. 6 the problem in drawing (a) (design #1) is the same as the problem in drawing (b) (the part has been flipped over). Similarly, the problem in drawing (c) (the stiff layer expanding relative to the compliant layer) is the same as that in (b) because the problem itself is driven by a relative strain mismatch between the layers. Finally, the problem in drawing (d) (which is design #2) is the opposite loading case as that in drawing (c). Thus, design #2 is simply the opposite loading case as design #1. Both designs have the same value for Gss as predicted by the residual stress model. However, a fracture analysis of design #2 predicts interpenetration of the crack faces, where for design #1 the crack faces experience a positive relative normal displacement. The difference in the two cases is demonstrated by the values of \|/ss (the steady-state value of \|/ defined in eq. (6)) given in Fig. 6. Design #1 has a value of $\backslash\backslash f_{ss} = 79°$, designating a positive Ki, and design #2 has a value of $\backslash|/ss = 101°$, designating a negative Ki. The physical significance of this result is that design #2 will be more delamination resistant than design #1. A delamination crack for design #2 will have its crack faces pressed together while they attempt to slide relative to one another. Frictional forces will serve to increase G_c for this case.

Also, the true steady-state energy released by a delamination crack for design #2 would be less than the calculated Gss because the contribution to Gss from crack face interpenetration would not be allowed in an actual part. Symmetry arguments have thus shown that for a simple two-layer case, the order in which layers are deposited can affect the delamination resistance of manufactured parts.

Figure 7 provides a plot of normalized G vs. a/h for debonding along the midplane of a four-layer part made of alternating layers of two materials with a modulus ratio of 1:3. Each layer has the same thickness, h, and has experienced the same free thermal contraction (characterized by aAT) relative to the layer below it. Although a steady-state analysis is as applicable to this case as it is for the two-layer cases, in the four-layer problem the debonded ends are not stress free. As the plot indicates, the energy release rate for the four-layer case reaches a predictable steady-state value within a distance of about 2h. In general, for deposited multi-layers experiencing debonding on any one interface, the crack length over which a steady-state is achieved should be on the order of the thickness of the thicker debonded section.

The difference in the behavior of G as a function of crack length for this case is evidenced by a local peak in G for short cracks. G_{ss} is not the maximum G for all crack lengths. This short crack peak is not related to the singular character of the stresses at the intersection of a fully bonded interface and the free edge (see the discussion related to Fig. 5). It is instead due to the low normalized G_{ss} for this case. For short cracks, the asymptotic behavior is the same for a given material combination and strain mismatch (regardless of the number and thickness of the layers). Thus, the short crack behavior of G vs. a for this problem is the same as that for the two-layer case shown in Fig. 4. The steady-state energy release rate for long cracks is relatively small for this case, however. The result is that the short crack G behavior overshoots the steady-state G value in the short crack limit. The low value observed for G_{SS} in this case is a consequence of the shape of the debonded halves of the four-layer part The energy released by debonding along the midplane is due to a mismatch in free thermal strain along the interface. Because each layer contracts relative to the one below it, the two debonded portions of this part are curved. The curvature of the debonded pieces decreases the strain mismatch along the interface (by decreasing the length of the top of the bottom two layers and by increasing the length of the bottom of the top two layers). The result is an unusually low G_{ss}.

The existence of a short crack maximum in G is not unique to this case. For example, it also occurs for the case of a single compliant layer debonding from the bottom of this four-layer part. In Fig. 8 the normalized energy release rate for this case is plotted as a function of normalized crack length. The very low value of Gss for this case results in a short crack peak in G that is comparatively large in magnitude. Figure 9 provides a plot of normalized energy release rates for the case of a single stiff layer debonding from this four-layer part. Because the steady-state G for this case is relatively large, G_{ss} is the maximum G over all crack lengths. In general, if

it is important to prevent the extension of small delamination cracks, it is necessary to consider the existence of short crack maxima in G such as those exhibited in Figs. 7 and 8. However, because the phenomenon is a consequence of low G^ values, it would generally not affect delamination behavior on critical interfaces (where, assuming G_c values are comparable, Gss values are high). Concern over short crack maxima in G should thus be limited to the analysis of comparatively brittle interfaces where a low energy release rate can still result in delamination.

The behavior of G as a function of crack length for four-layer cases with stiffness mismatches other than 1:3 generally follows that demonstrated in Figs. 7,8 and 9. For the case of a four-layer part with no stiffness mismatch, short crack maxima in G are exhibited for debonding along the midplane and for debonding of a single layer. The problem of debonding along the midplane of a four-layer part with no stiffness mismatch offers further insight into the relationship between low Gss values and observed short crack peaks in energy release rates. The curvature of the debonded portions in this four-layer problem is the only physical difference between it and a two-layer configuration with no stiffness mismatch and the same total thickness, H (see Fig. 3). This curvature leads to a steady-state energy release rate (look ahead to Table 2) that is one-fourth of the steady-state energy release rate for the analogous two-layer problem. The four-layer problem exhibits a short crack peak in G. The two-layer problem does not

Figure 10 provides a plot of the mode parameter *y* vs. a/h for the four-layer case depicted in Fig. 7. Because the problem itself is a steady-state one, a steady-state value of y is reached at essentially the same rate that G_{ss} is reached in the plot of Fig. 7. The steady-state value of \|f is very close to 90°, indicating primarily tangential displacement of the crack faces. As the symmetric crack tips approach one another, the value of *f* becomes greater than 90°. Values of \|/ greater than 90° do not imply crack face interpenetration (in fact, no large-scale crack face contact exists for these cases). This is due to an offset between the phase of K and the phase of the crack face displacements due to e effects. In any event, the displacements of the crack faces for this case are primarily tangential for all crack lengths.

Figure 11 provides an illustration analogous to that given in Fig. 6, demonstrating how symmetry arguments can be used to relate delaminations in two different four-layer part "designs." Using the symmetry arguments made in the discussion of Fig. 6, it can be shown that delamination of a single compliant layer off the bottom of design #1 is equivalent to the delamination of a single compliant layer off the top of design #2 with the loading reversed. Thus G_{ss} values are the same but the sign of Ki is reversed. The crack face interpenetration associated with design #2, though physically impossible, indicates that the delamination event associated with design #2 would be much less likely to occur than that associated with design #1 (assuming equal free thermal strain mismatches). Figure 12 gives a summary of G_{ss} and $\|/_{ss}$ values for these two designs for the propagation of a delamination crack along any of the three material interfaces. If a simple criterion is applied that if delamination occurs, it will occur on the interface with the largest Gss value and a

positive value of Ki, then debonding would be predicted to occur along the bottom interface for design #2. The case for design #1 is not as clear. Part debonding could occur at the midplane or along the bottom interface. Although debonding along the bottom interface would be associated with a positive Ki, the magnitude of its Gss is lower than that for debonding along the midplane interface, where Ki is essentially equal to zero. A comparison with mode-dependent G_c values would be required to offer more insight in this case. In any event, it is apparent from symmetry arguments that the ordering of material layers can have an effect on the location and the likelihood of debonding in a deposited multi-layer part.

In order to predict multi-layer delamination resistance, values of Gss and Vss are needed for comparison with ^-dependent G_c values. Tables 1 and 2 offer a summary of normalized G$& and Yss values for two-layer and four-layer deposited bi-material configurations up to a stiffness mismatch of 1:40. Cases where Gss is not the maximum energy release rate are indicated and the maximum normalized G value is provided. For the two cases in Table 1 having a stiffness mismatch, the values of $\|/_{SS}$ are for a compliant layer deposited onto a stiff layer. The values of Vss presented in Table 2 for a single layer debonding from a four-layer part are for that layer debonding from the bottom of the part These are the cases that exhibit large-scale opening of the crack faces.

Conclusions

This study involves modeling delamination problems in materials and parts manufactured by successive deposition of material layers. The delamination-problem is modeled as an interfacial fracture problem, exploiting its steady-state behavior for long delamination cracks. This approach greatly simplifies understanding. The steady-state delamination energy release rate, Gss, can be calculated directly from a residual stress model. Also, the parameter G_{ss} is ideal for use in determining critical interfaces where debonding may occur and can serve as a guide for the design of delamination-resistant multi-layer configurations. For example, it could be used to determine, for a given combination of materials in alternating layers, if a particular distribution of layer thicknesses will decrease the likelihood of delamination along an identified critical interface.

Finite element modeling of the fracture problem associated with delamination has also been carried out in order to verify the applicability of the steady-state analysis and to extract crack extension mode and crack face contact information. The results show that the steady-state analysis applies over a large range of crack lengths and part dimensions. The finite element results show that G_{ss} can be used to determine the susceptibility of an interface to residual stress-driven delamination; however, for cases exhibiting low G_{ss} values, G for short cracks can exceed G_{ss}. Thus, care must be taken in using the requirement that $G_c > G_{SS}$ in applications where it is important to prevent the extension of small delamination craCks on brittle interfaces. G_{SS} values and symmetry arguments have been used to show that the ordering of layers can change the

location where delamination is most likely to occur and, in doing so, it can change the susceptibility of a part to delamination.

Acknowledgment

The authors gratefully acknowledge the Office of Naval Research, Grant No. N00014-94-1-0183, the Carnegie Mellon University Department of Mechanical Engineering, the University Research Initiative at the University of California at Santa Barbara, Grant No. N00014-92-J-1808 and the Engineering Design Research Center, an Engineering Research Center of the National Science Foundation, Grant No. EEC-8943164. The authors would also like to thank Lee Weiss and Fritz Prinz for their thoughts and insights related to this research.

References

Bogy, D.B. (1971) Two edge-bonded elastic wedges of different materials and wedge angles under surface tractions. *J. Appl. Mech.,* 38, 377-386.

Crossman, F.W. and Wang, A.S.D. (1977) Stress field induced by transient moisture sorption in finite-width composite laminates. *J. Comp. Mat,* 12, 2-18.

Drory, M.D., Thouless, M.D. and Evans, A.G. (1988) On the decohesion of residually stressed thin films. *Acta MetalU* 36, 2019-2028.

Evans, A.G., Drory, M.D. and Hu, M.S. (1988) The cracking and decohesion of thin films. /. *Mater. Res.,* 3, 1043-1049.

Hein, V.L. and Erdogan, F. (1971) Stress singularities in a two-material wedge. *Int. J. Fract. Mech.,* 7, 317-330.

Herakovich, C.T. (1976) On thermal edge effects in composite laminates. *Int. J. Mech. ScL,* 18, 129-134.

Hutchinson, J.W. and Suo, Z. (1991) Mixed mode cracking in layered materials. *Advances in Applied Mechanics,* 28, (Edited by J.W. Hutchinson and T.Y. Wu), Academic Press.

Matos, P.P.L., McMeeking, R.M., Charalambides, P.G. and Drory, M.D. (1989) A method for calculating stress intensities in bimaterial fracture. *Int. J. Fract.,* 40, 235-254.

Merz, R., Prinz, F.B., Ramaswami, K., Terk, M., and Weiss, L.E. (1994) Shape deposition manufacturing. Proc. Solid Freeform Fabrication Symposium, H. Marcus, J.J. Beaman, J.W. Barlow, D.L. Bourell and R.H. Crawford eds., The University of Texas at Austin, August 1994, 1-8.

O'Brien, T.K. (1982) Characterization of delamination onset and growth in a composite laminate. ***Damage in Composite Materials,* ASTM STP 775,140-147.**

O'Brien, T.K., Raju, I.S. and Garber, D.P. (1986) Residual thermal and moisture influences on the strain energy release rate analysis of edge delamination. *J. Comp. Tech. Res.,* 8, 37-47.

Pagano, N.J. and Pipes, R.B. (1973) Stress field induced by transient moisture sorption in finite-width composite laminates. ***J. Comp. Mat.*****, 12, 2-19.**

Rice, J.R. (1988) Elastic fracture mechanics concepts for interfacial cracks. ***J. Appl. Mech.*****, 55, 98-103.**

Suo, Z. and Hutchinson, J.W. (1990) Interface crack between two elastic layers. ***Int. J. Fract,*** **43, 1-18.**

Thouless, M.D., Cao, H.C. and Mataga, P.A. (1989) Delamination from surface cracks in composite materials. ***J. Mat. ScL*****, 24, 1406-1412.**

Timoshenko, S. (1925) Bending and buckling of bimetal strips. ***J. Optical Soc. Am.*****, 11, 233-255.**

Wang, S.S. (1982) Fracture mechanics for delamination problems in composite materials. ***Progress in Science and Engineering of Composites*****, T. Hayashi, K. Kawata and S. Umekawa, Ed., Proc. ICCM-IV, Tokyo, 1982, 287-296.**

Wang, S.S. (1984) Edge delamination in angle-ply composite laminates. ***AIAA Journal,*** **22,256-264.**

Wang, S.S. and Choi, L, (1982) Boundary-layer effects in composite laminates (Parts 1 and 2). ***J. Appl. Mech.****y* **49, 541-560.**

Whitney, J.M. (1973) Free-edge effects in the characterization of composite materials. ***Analysis of the Test Methods for High Modulus Fibers and Composites*****, ASTM STP 521,167-180.**

TABLE 1

Steady-State G and \\f Values for Two Deposited Layers

Equal Layer Thickness and Equal Free Thermal Mismatch

Modulus Ratio	G_{ss}/G_o	Vss
1:1	1.0	90°
1:3	0.92	79°*
1:40	0.29	64°*

TABLE 2

Steady-State G and \\f Values for Four Deposited Layers

Two Alternating Materials, Equal Layer Thickness and Equal Free Thermal Mismatch

Modulus Ratio	Debond Case	Gss/Go	Gmax/Go	*Vss*
1:1	IVfidplane Debond	0.249	0.35	90°
	1 Layer Debond	0.360	0.42	63°**
1:3	IVfidplane Debond	0.321	0.35	90°
	Compliant Layer Debond	0.182	0.27	60°**
	Stiff Layer Debond	0.555	—	68°**
1:40	IVfidplane Debond	0.936	—	89°
	Compliant Layer Debond	0.0183	0.077	59°**
	Stiff Layer Debond	0.984	—	84°**

Notes for Tables 1 and 2:

Gmax values are provided for cases where G_{ss} * G_{max}»

G_o is defined in eq. (8), \S is defined in eq. (6) and $\|/_{ss}$ values are for cases with vi=V2=l/3.

* These $\|f_{ss}$ values are for a compliant layer deposited onto a stiff layer.

** These y_{ss} values are for a single layer debonding from the bottom of the part.

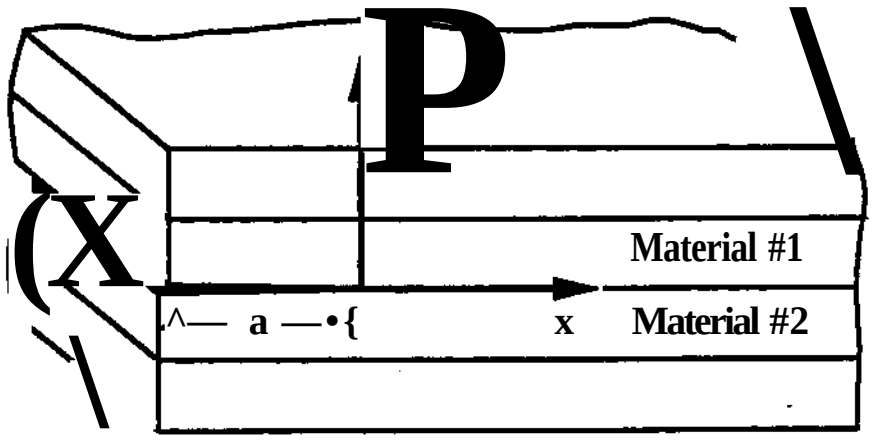

Figure 1 Delamination Crack Propagating Along the Midplane of a Four-layer Part

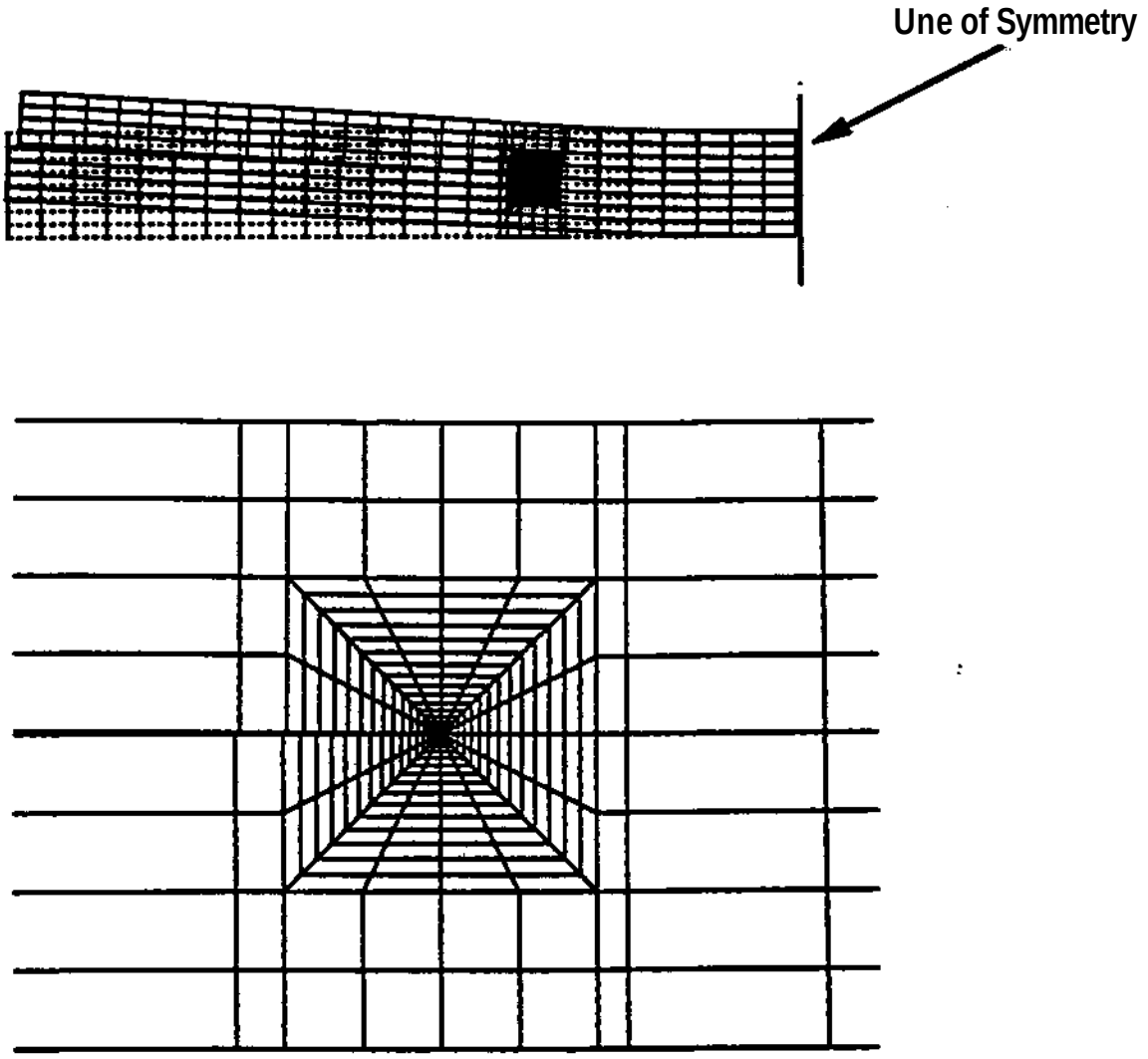

Rgure 2 Far-field and Near-tip Finite Element Meshes

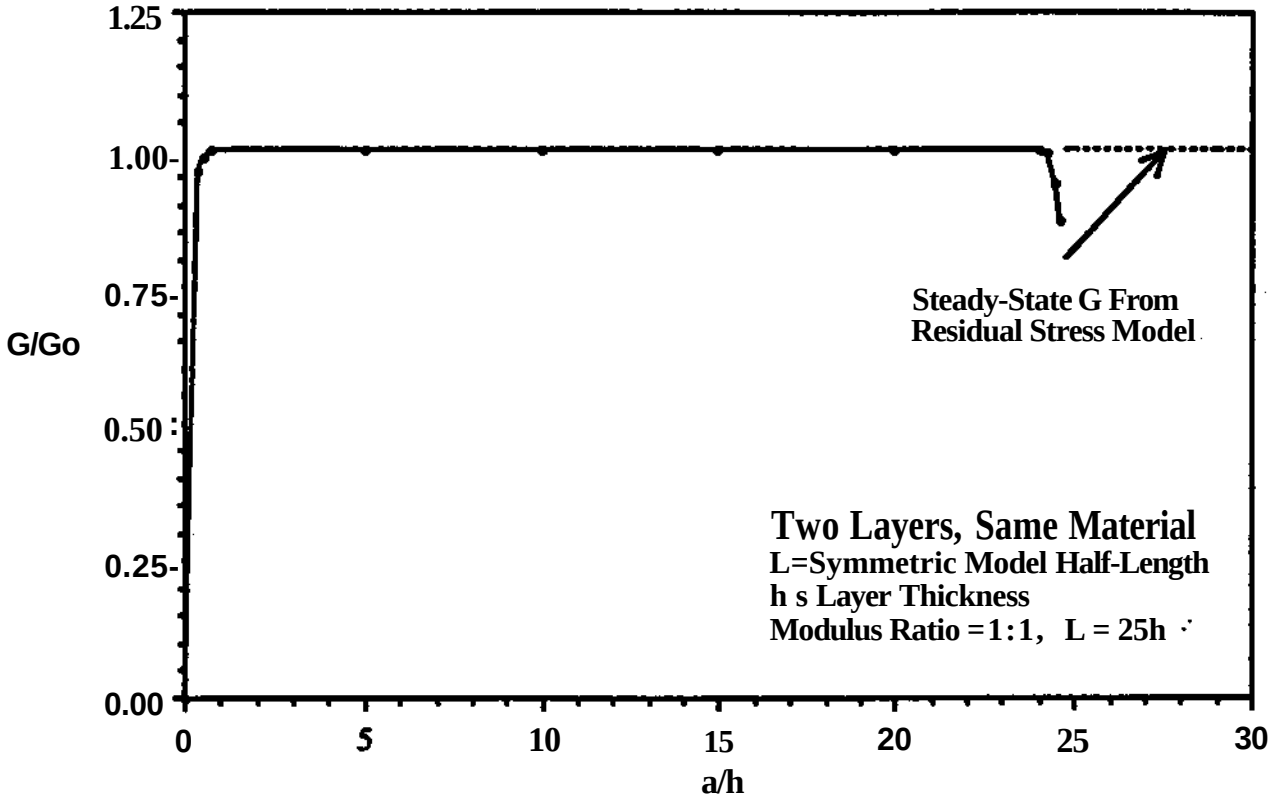

Figure 3 Nonnalized G vs. Normalized Crack Length for Two Layers with Equal Elastic Moduli

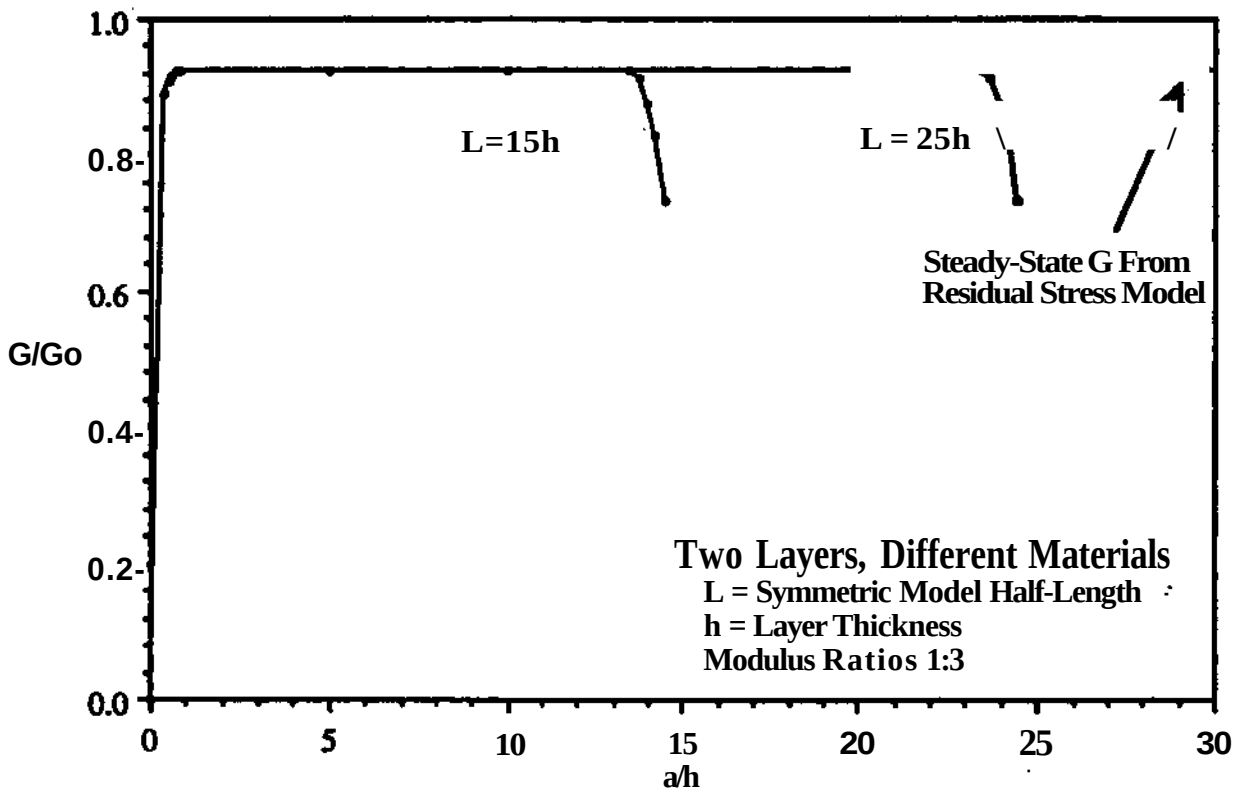

Figure 4 Normalized G vs. Normalized Crack Length for Two Layers with a Modulus Ratio of 1:3

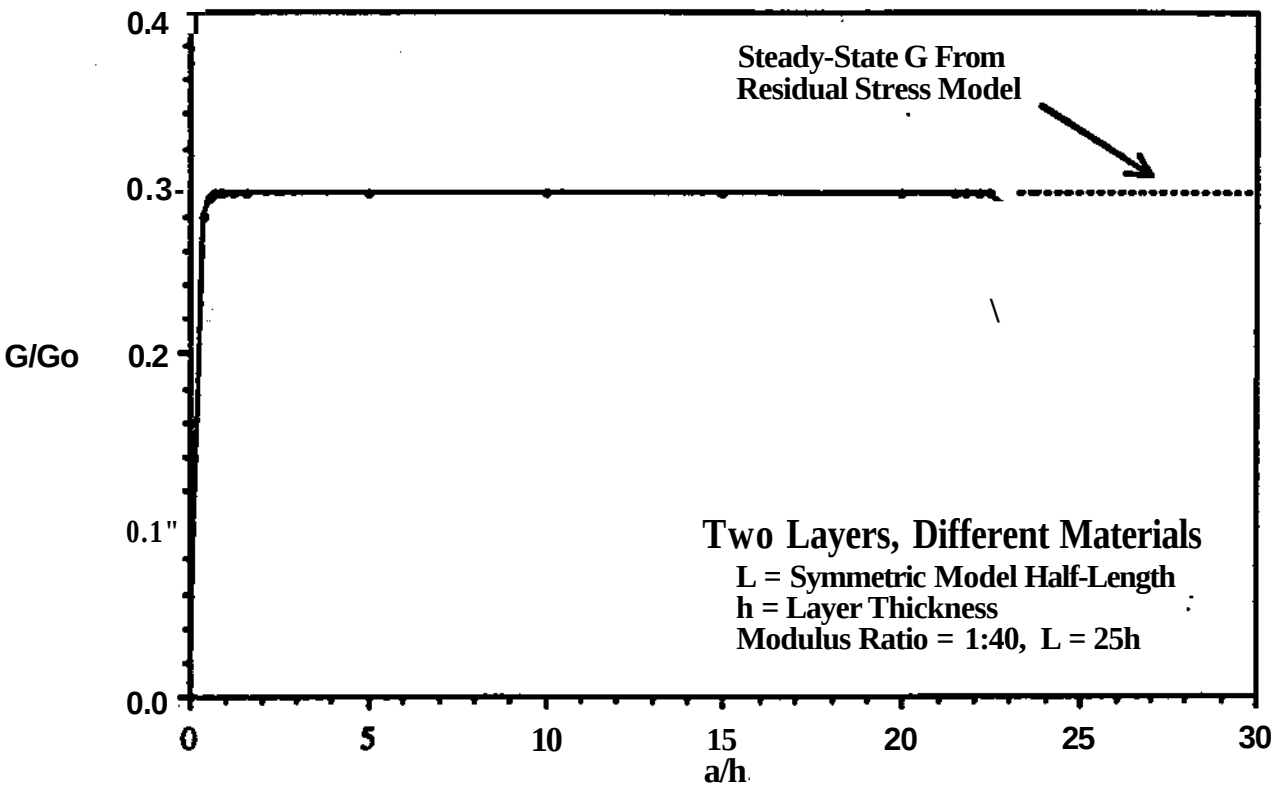

Figure 5 Nonnalized G vs. Nonnalized Crack Length for Two Layers with a Modulus Ratio of 1:40

Design #1

Modulus Ratio = 1:3 $\psi_{ss} = 79°$

(a)

(b)

(c)

Design #2

Modulus Ratio = 1:3 y^ = 101°

Crack Faces Interpenetrate on a Large Scale

(d)

Figure 6 Ordering and Symmetry Arguments for Two-Layer Parts

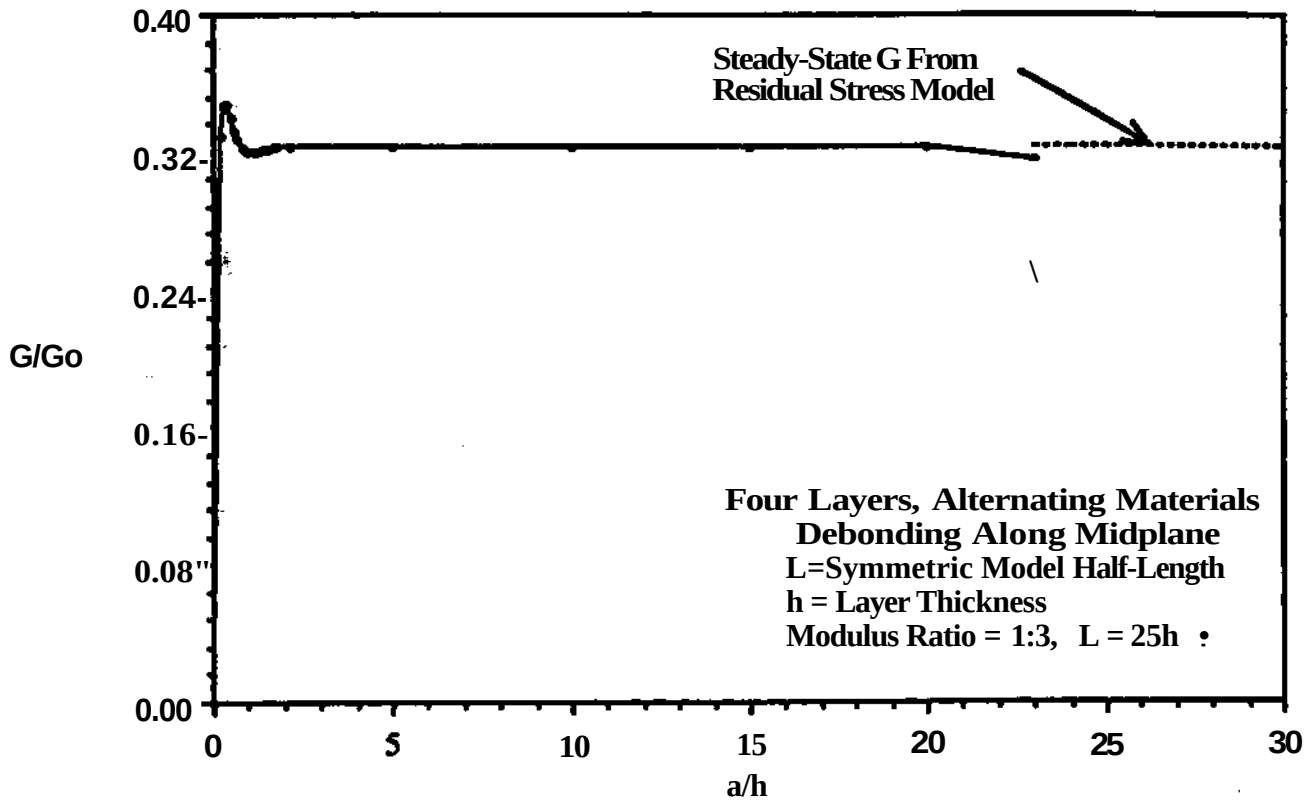

Figure 7 Normalized G vs. Normalized Crack Length for Four Layers with Debonding Along the Midplane (Modulus Ratio of 1:3)

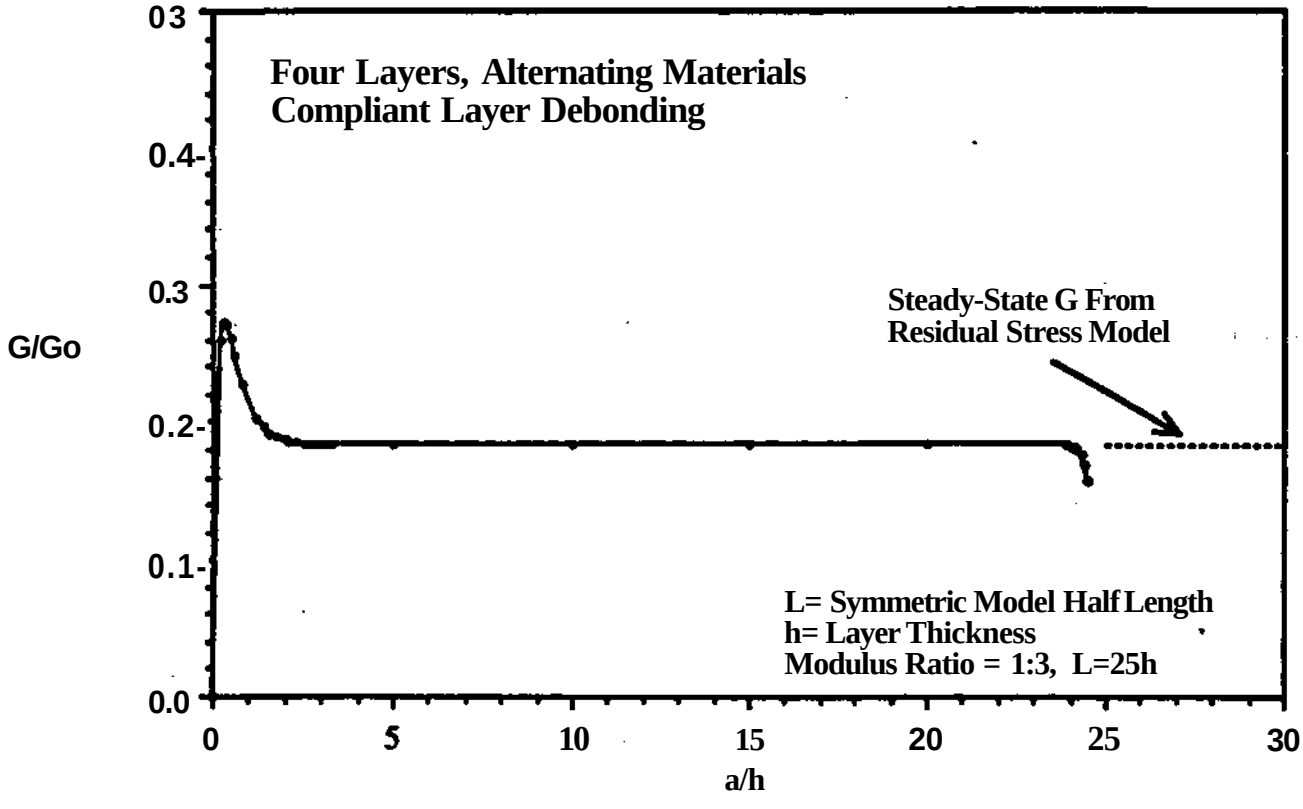

Figure 8 Nonnalized G vs. Nonnalized Crack Length for a Single Compliant Layer Debonding from the Bottom of a Four-Layer Part (Modulus Ratio of 1:3)

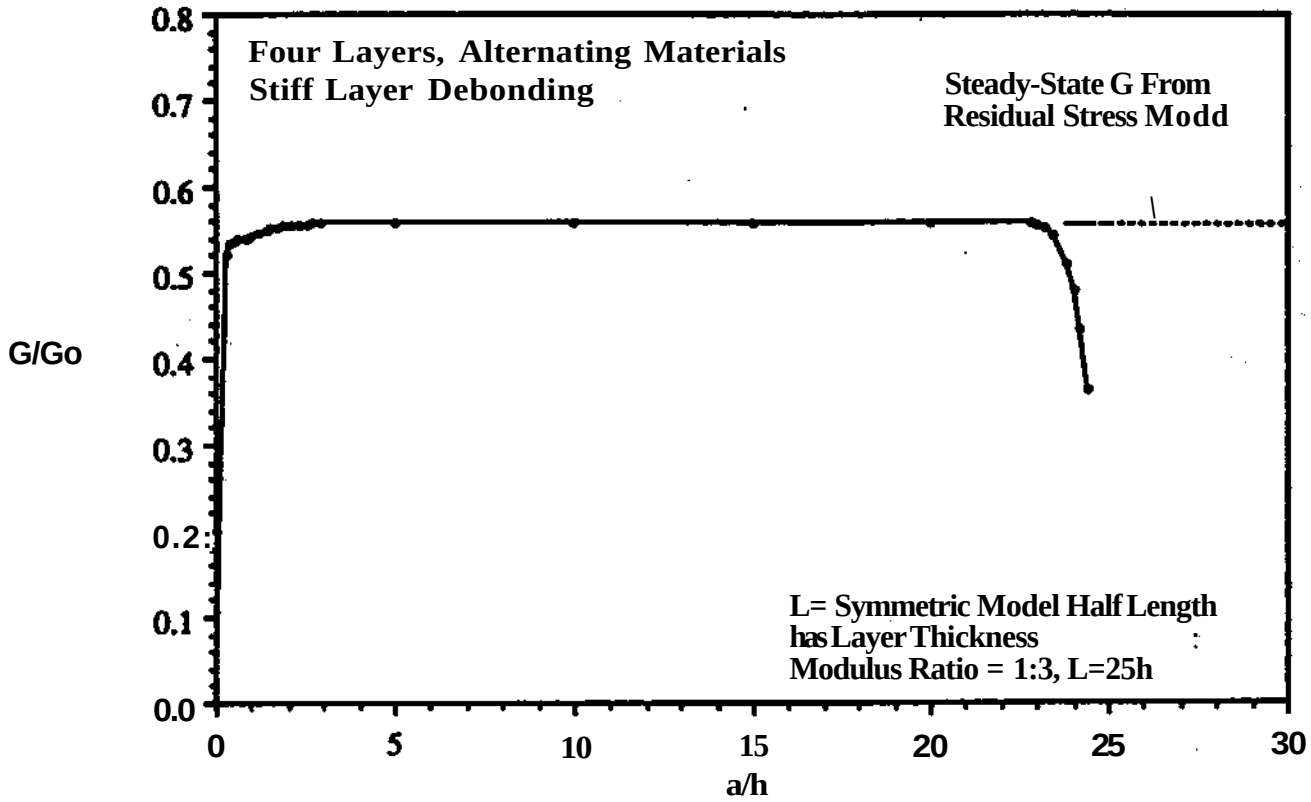

Figure 9 Normalized G vs. Normalized Crack Length for a Single Stiff Layer Debonding from the Bottom of a Four-Layer Part (Modulus Ratio of 1:3)

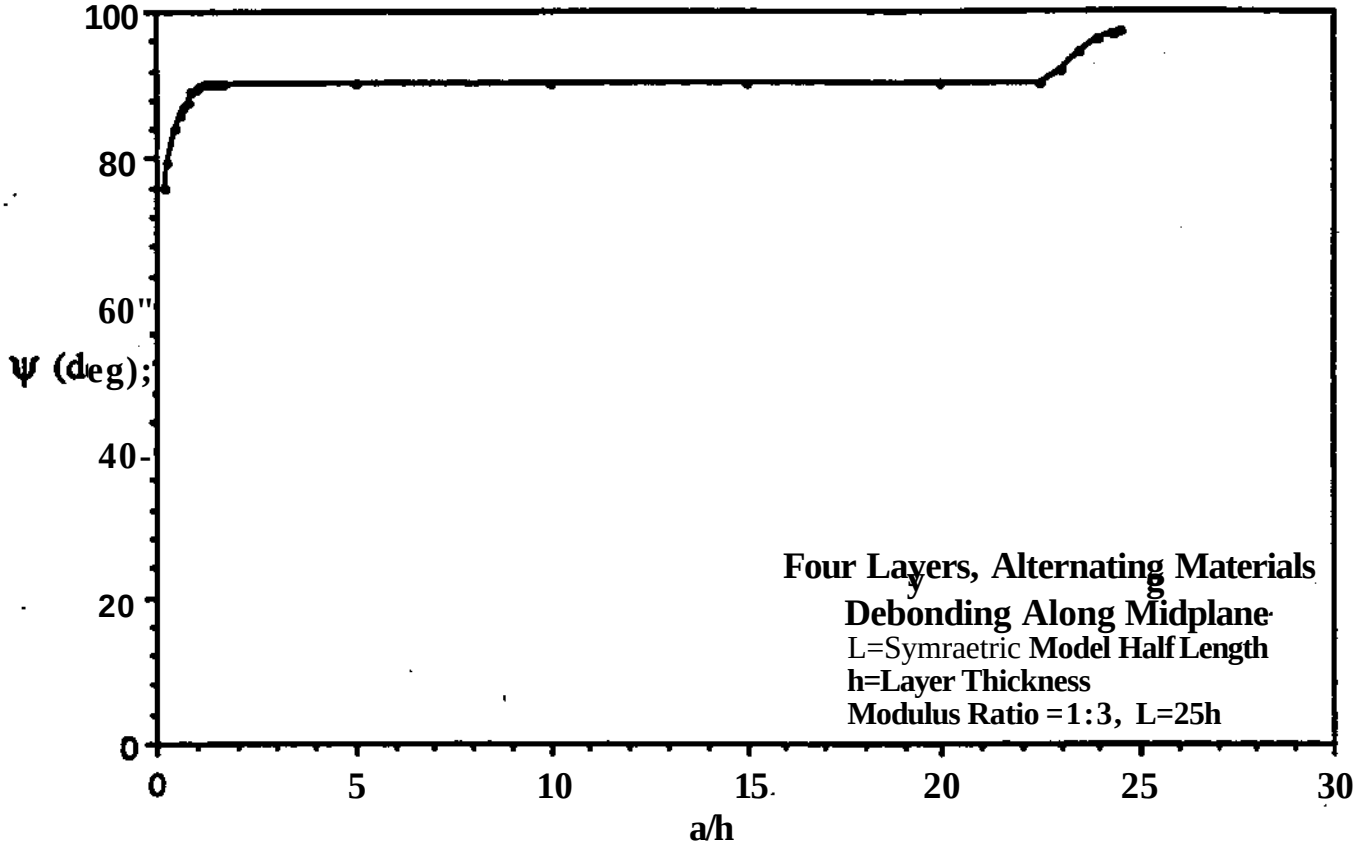

Figure 10 v vs. Normalized Crack Length for Four Layers with Debonding Along the Midplane (Modulus Ratio of 1:3, vi = V2 = 1/3)

Design #1

Modulus Ratio=1:3 Vss = 60°

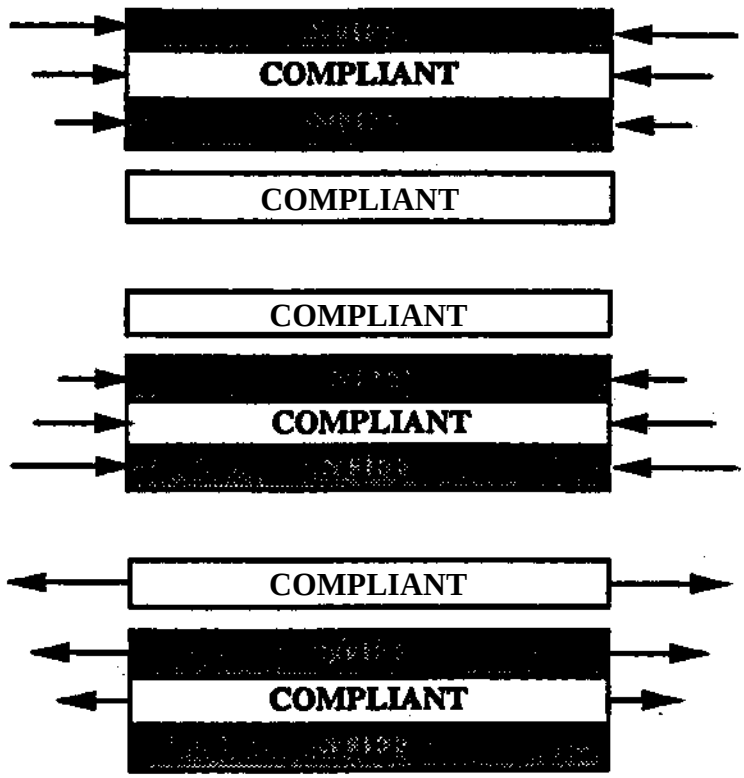

Design #2

Modulus Ratio = 1:3 ^ = 1 2 0 °

Crack Faces Interpenetrate on a Large Scale

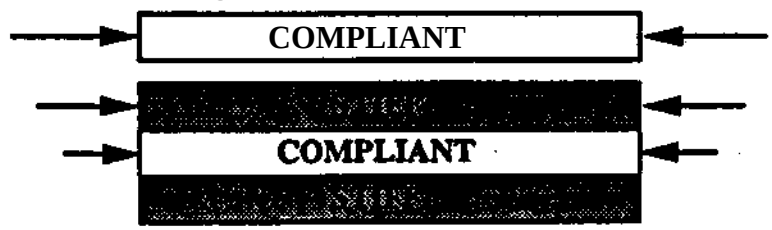

Figure 11 Ordering and Symmetry Arguments for Four-Layer Parts (Modulus Ratio of 1:3)

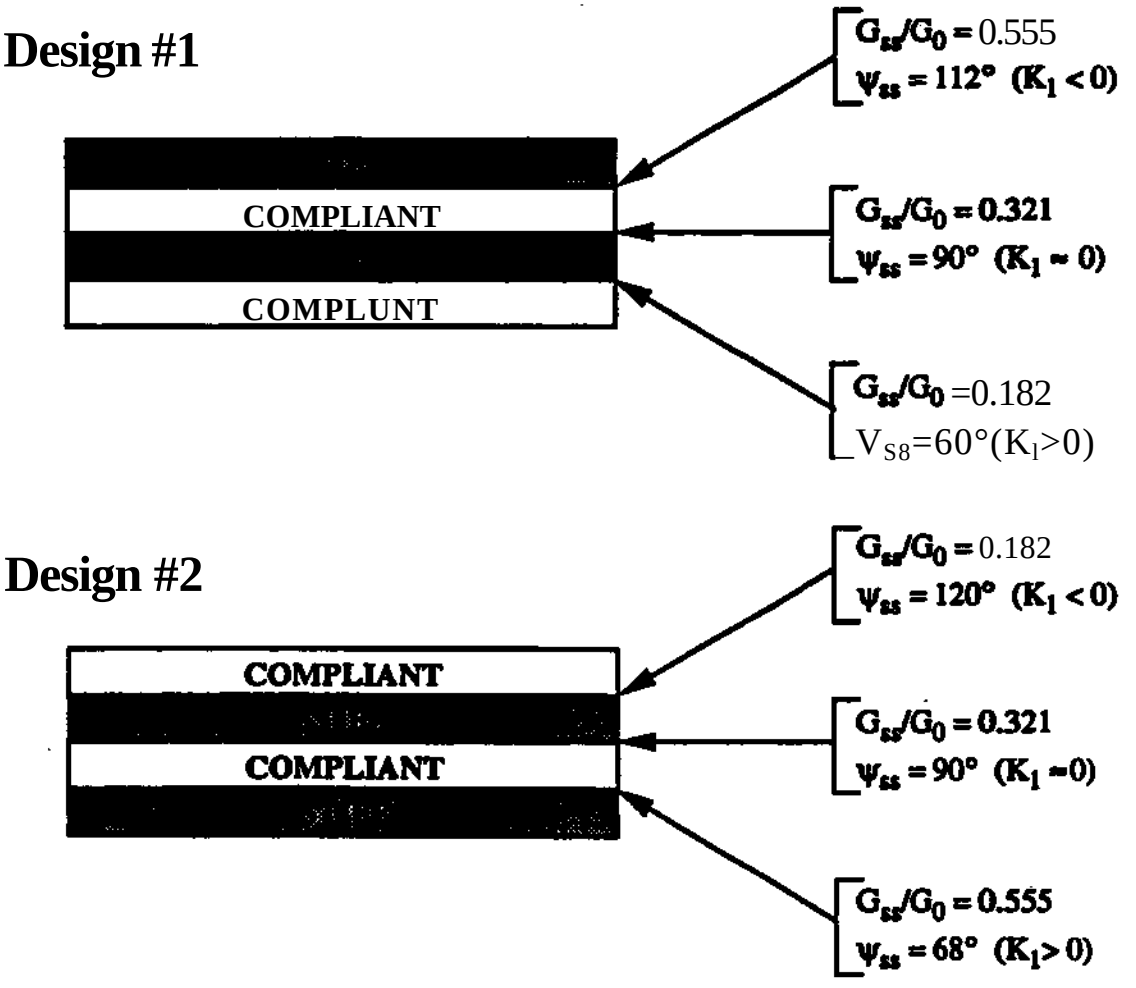

Figure 12 Comparison of Delamination Behavior of Two Four-Layer Part Designs (Modulus Ratio of 1:3)